

SPECTROSCOPIC CONFIRMATION OF THREE z -DROPOUT GALAXIES AT $z = 6.844 - 7.213$:
DEMOGRAPHICS OF LYMAN-ALPHA EMISSION IN $z \sim 7$ GALAXIES[‡]

YOSHIKI ONO¹, MASAMI OUCHI^{2,3}, BAHRAM MOBASHER⁴, MARK DICKINSON⁵, KYLE PENNER⁶,
KAZUHIRO SHIMASAKU^{1,7}, BENJAMIN J. WEINER⁸, JEYHAN S. KARTALTEPE⁵, KIMIHIKO NAKAJIMA¹,
HOOSHANG NAYYERI⁴, DANIEL STERN⁹, NOBUNARI KASHIKAWA¹⁰, AND HYRON SPINRAD¹¹

Accepted for publication in ApJ

ABSTRACT

We present the results of our ultra-deep Keck/DEIMOS spectroscopy of z -dropout galaxies in the SDF and GOODS-N. For 3 out of 11 objects, we detect an emission line at $\sim 1\mu\text{m}$ with a signal-to-noise ratio of ~ 10 . The lines show asymmetric profiles with high weighted skewness values, consistent with being Ly α , yielding redshifts of $z = 7.213, 6.965,$ and 6.844 . Specifically, we confirm the $z = 7.213$ object in two independent DEIMOS runs with different spectroscopic configurations. The $z = 6.965$ object is a known Ly α emitter, IOK-1, for which our improved spectrum at a higher resolution yields a robust skewness measurement. The three z -dropouts have Ly α fluxes of $3 \times 10^{-17} \text{ erg s}^{-1} \text{ cm}^{-2}$ and rest-frame equivalent widths $\text{EW}_0^{\text{Ly}\alpha} = 33 - 43\text{\AA}$. Based on the largest spectroscopic sample of 43 z -dropouts that is the combination of our and previous data, we find that the fraction of Ly α -emitting galaxies ($\text{EW}_0^{\text{Ly}\alpha} > 25\text{\AA}$) is low at $z \sim 7$; $17 \pm 10\%$ and $24 \pm 12\%$ for bright ($M_{\text{UV}} \simeq -21$) and faint ($M_{\text{UV}} \simeq -19.5$) galaxies, respectively. The fractions of Ly α -emitting galaxies drop from $z \sim 6$ to 7 and the amplitude of the drop is larger for faint galaxies than for bright galaxies. These two pieces of evidence would indicate that the neutral hydrogen fraction of the IGM increases from $z \sim 6$ to 7, and that the reionization proceeds from high- to low-density environments, as suggested by an inside-out reionization model.

Subject headings: cosmology: observations — galaxies: formation — galaxies: evolution — galaxies: high-redshift —

1. INTRODUCTION

Over the last two years, we have witnessed an explosion of activities aimed at searching for very high redshift ($z > 7$) galaxies. This has been made possible by the installation of the Wide-Field Camera 3 (WFC3) on-board the Hubble Space Telescope (e.g., Oesch et al.

2010, 2011; Bouwens et al. 2010a, 2011b,a; McLure et al. 2010, 2011; Wilkins et al. 2010, 2011; Bunker et al. 2010; Yan et al. 2010, 2011; Lorenzoni et al. 2011), the Hawk-I instrument on the Very Large Telescope (VLT; Castellano et al. 2010a,b), and improvement in the red-end sensitivity of the Suprime-Cam on the Subaru telescope (Ouchi et al. 2009). These studies have identified over a hundred candidates at $z > 6.5$ through the Lyman break drop-out technique (e.g., Steidel et al. 1996; Giavalisco 2002), showing a decrease in the number density of bright high-redshift galaxies with redshift (e.g., Ouchi et al. 2009; McLure et al. 2010; Castellano et al. 2010a; Bouwens et al. 2010a; Wilkins et al. 2010), bluer UV continua (e.g., Bouwens et al. 2010b)¹³, and relatively smaller stellar masses compared to lower redshift galaxies selected by similar techniques (e.g., Labbé et al. 2010; Schaerer & de Barros 2010; Finkelstein et al. 2010; Ono et al. 2010). Study of the intrinsic properties of high-redshift galaxies at epochs close to the dark ages is essential for understanding one of the most outstanding questions in modern astronomy - when did the Universe become reionized and what sources were responsible for it? This can be accomplished by studying the state of the inter-galactic medium (IGM) through estimates of the ionizing photon budget and Lyman α escape fraction.

Several independent studies of the reionization process in recent years have yielded different results. By measuring the polarization of the cosmic background radiation, Dunkley et al. (2009) estimated the optical

ono_at_astron.s.u-tokyo.ac.jp

¹ Department of Astronomy, Graduate School of Science, The University of Tokyo, Tokyo 113-0033, Japan

² Institute for Cosmic Ray Research, University of Tokyo, Kashiwa 277-8582, Japan

³ Institute for the Physics and Mathematics of the Universe (IPMU), TODIAS, University of Tokyo, 5-1-5 Kashiwanoha, Kashiwa, Chiba 277-8583, Japan

⁴ Department of Physics and Astronomy, University of California, Riverside, CA, 92521, USA

⁵ National Optical Astronomical Observatories, Tucson, AZ 85719, USA

⁶ Department of Astronomy, University of Arizona, 933 N. Cherry Ave., Tucson, AZ 85721, USA

⁷ Research Center for the Early Universe, Graduate School of Science, The University of Tokyo, Tokyo 113-0033, Japan

⁸ Steward Observatory, University of Arizona, 933 N. Cherry Avenue, Tucson, AZ 85721, USA

⁹ Jet Propulsion Laboratory, California Institute of Technology, 4800 Oak Grove Drive, Pasadena, CA 91109, USA

¹⁰ Optical and Infrared Astronomy Division, National Astronomical Observatory of Japan, 2-21-1, Osawa, Mitaka, Tokyo, 181-8588, Japan

¹¹ Department of Astronomy, University of California, Berkeley, CA 94720, USA

[‡] Based on data obtained with the Subaru Telescope and the W. M. Keck Observatory. The Subaru Telescope is operated by the National Astronomical Observatory of Japan. The W. M. Keck Observatory is operated as a scientific partnership among the California Institute of Technology, the University of California, and the National Aeronautics and Space Administration.

¹³ See also Dunlop et al. (2011), who question this result.

depth to reionization and concluded that, if it was a sudden event, reionization occurred at $z = 11.0 \pm 1.4$ (see also, Komatsu et al. 2011; Larson et al. 2011). However, investigating the spectra of SDSS quasars, Fan et al. (2006) studied the evolution of the Gunn-Peterson optical depth and demonstrated that the IGM reionization may have ended as late as $z \sim 6$. The result from this study is questioned by Goto et al. (2011), who have shown that for quasars at $z > 6$, a statistically large number is needed in $\Delta z = 0.1$ bins to constrain cosmic variance and trace the evolution of the optical depth.

Another useful tool for studying reionization is the Lyman α luminosity function of high-redshift galaxies selected by narrow-band imaging (e.g., Hu et al. 1998; Rhoads et al. 2000); these galaxies are called Lyman Alpha Emitters (LAEs). Since neutral hydrogen in the IGM resonantly scatters Ly α photons, the transmission of Ly α is sensitive to the ionization state of the IGM. Therefore, we expect a decrease in the number density of LAEs close to the reionization epoch (e.g., Haiman & Spaans 1999; Malhotra & Rhoads 2004; Santos et al. 2004; Mesinger et al. 2004; Stern et al. 2005; Haiman & Cen 2005; Furlanetto et al. 2006; McQuinn et al. 2007; Dijkstra et al. 2007; Kobayashi et al. 2007; Mesinger & Furlanetto 2008; Iliiev et al. 2008; Dayal et al. 2008, 2009, 2011). Ouchi et al. (2010) found a decrease in the Ly α luminosity function of LAEs, corresponding to an upper limit of the IGM neutral fraction $x_{\text{HI}} \lesssim 0.2 \pm 0.2$ at $z = 6.6$, which indicates that the major reionization process took place at higher redshift. This result has been further supported by Kashikawa et al. (2011), who studied the evolution of the LAE luminosity function in the Subaru Deep Field (SDF; Kashikawa et al. 2004) and found an increase in the neutral fraction of the IGM from $z = 5.7$ to 6.5. Nakamura et al. (2011) have also found a large deficit in the number density of $z = 6.5$ LAEs in the SSA22 field, and attributed it to significant field-to-field variance of the neutral fraction of the IGM. The effect of cosmic variance was quantified by Ouchi et al. (2010), who claimed a factor of 2–10 range in the number density of LAEs in an extensive survey covering an area of 1 deg².

Measuring the fraction of LAEs among Lyman-break Galaxies (LBGs; Giavalisco 2002), the Ly α fraction, provides complementary information to understand the reionization process (e.g., Stark et al. 2010). Since LBGs are selected over a broader range of redshifts compared to observations with a narrow-band filter, their number density is less sensitive to cosmic variance. Searching for Ly α emission from samples of LBGs with available spectra at $4 < z < 6$, Stark et al. (2011) showed that lower luminosity LBGs have larger Ly α fractions, and that the fraction increases with redshift (see also, Vanzella et al. 2009; Stark et al. 2010; Douglas et al. 2010). However, it is not yet clear if this trend continues $z > 6$. To explore this, we require spectroscopy of dropout candidates at $z \sim 7$.

The real challenge in estimating the number density of $z > 6$ galaxies and the intensity of ionizing Ly α photons is the spectroscopic confirmation of these candidates. They are extremely faint, and the only detectable feature is Ly α emission shifted to near-infrared wavelengths (e.g., Iye et al. 2006; Lehnert et al. 2010; Fontana et al.

2010; Vanzella et al. 2011). Despite significant efforts to spectroscopically confirm $z > 6$ candidates, the number of confirmed sources is still very limited. Fontana et al. (2010) reported the detection of one LBG with Ly α emission at $z = 6.97$ in ultra-deep spectroscopy of seven z -dropout candidates selected from VLT/Hawk-I imaging of the Great Observatories Origins Deep Survey’s southern (GOODS-S) field (Castellano et al. 2010a). They found a significant decline in the fraction of LBGs with Ly α emission between $z \sim 6$ and 7, reversing the increasing trend with redshift found at $z < 6$. Furthermore, Vanzella et al. (2011) spectroscopically confirmed two z -dropout galaxies at $z \approx 7.1$ selected from VLT/Hawk-I imaging of the BDF4 field (Castellano et al. 2010b). With the small number of z -dropout galaxies with available spectroscopic redshifts, any measure of their Ly α photon budget or number density will be seriously affected by statistical uncertainties and cosmic variance.

In this study we present results from ultra-deep spectroscopy with Keck/DEIMOS for a sample of 11 z -dropout galaxies. To maximize the spectroscopic success, we designed the photometric survey to identify dropout candidates at the bright end of the UV luminosity function. The aim is to derive the fraction of LBGs with Ly α emission and to study its evolution to $z \sim 7$.

In the next section we present the photometric selection of z -dropout candidates which are the targets for our spectroscopic observations here. The spectroscopic observations are described in Section 3. This is followed by redshift identification and the measurement of spectroscopic properties in Section 4. In Section 5 we discuss the implications for reionization. The conclusions are presented in Section 6. Throughout this paper, we use magnitudes in the AB system (Oke & Gunn 1983) and assume a flat universe with $(\Omega_{\text{m}}, \Omega_{\Lambda}, h) = (0.3, 0.7, 0.7)$.

2. PHOTOMETRIC SELECTION OF z -DROPOUT CANDIDATES

In order to achieve successful spectroscopy of high redshift LBGs, we need to identify a sample of bright candidates. However, the bright end of the luminosity function exponentially decreases. Therefore, we need to cover a large area to find a sufficient number of LBGs bright enough for spectroscopy.

We carried out a wide-area photometric survey aimed at identifying z -dropout galaxies (i.e., galaxy candidates at $z \sim 7$) using Suprime-Cam on the Subaru telescope, outfitted with a custom-made filter (y -band) with effective wavelength at 1 μ m (Ouchi et al. 2009). This combination is ideal for identifying the bright population of LBGs at high redshifts. We covered an area of 1568 arcmin² to $y \simeq 26.0$ mag (4σ limit) for two fields: the SDF and the GOODS northern field (GOODS-N; Giavalisco et al. 2004). We identified 22 z -dropout candidates with $y = 25.4 - 26.1$ mag, i.e., $M_{\text{UV}} < -21$. This includes a galaxy which was already identified to be at a spectroscopic redshift of 6.96 (Iye et al. 2006). These provide the targets for the spectroscopic observations in this paper.

3. SPECTROSCOPIC OBSERVATIONS

We used the DEep Imaging Multi-Object Spectrograph (DEIMOS; Faber et al. 2003) at the Nasmyth focus of the 10 m Keck II telescope to perform spectroscopic

TABLE 1
SUMMARY OF OBSERVATIONS WITH KECK/DEIMOS.

Mask ID	Field	Date (UT)	Total Exposure [sec]	N_z^\dagger	grating [lines mm ⁻¹]	central wavelength [Å]	filter
SDFZD1B	SDF	2010 February 13	19350	5	830	9000	OG550
SDFZD3	SDF	2010 April 14 – 15	30000	2	830	9000	OG550
SDFZD4	SDF	2010 April 15	7200	4	830	9000	OG550
GNZD1B	GOODS-N	2010 February 13, April 14-15	18000	2	830	9000	OG550
HDF11C	GOODS-N	2011 April 1 – 2	14600	2	600	7500	GG455
HDF11D	GOODS-N	2011 April 3	7200	2	830	8100	OG550

[†] Numbers of observed z -dropouts. Some objects were observed on multiple masks (See Table 2).

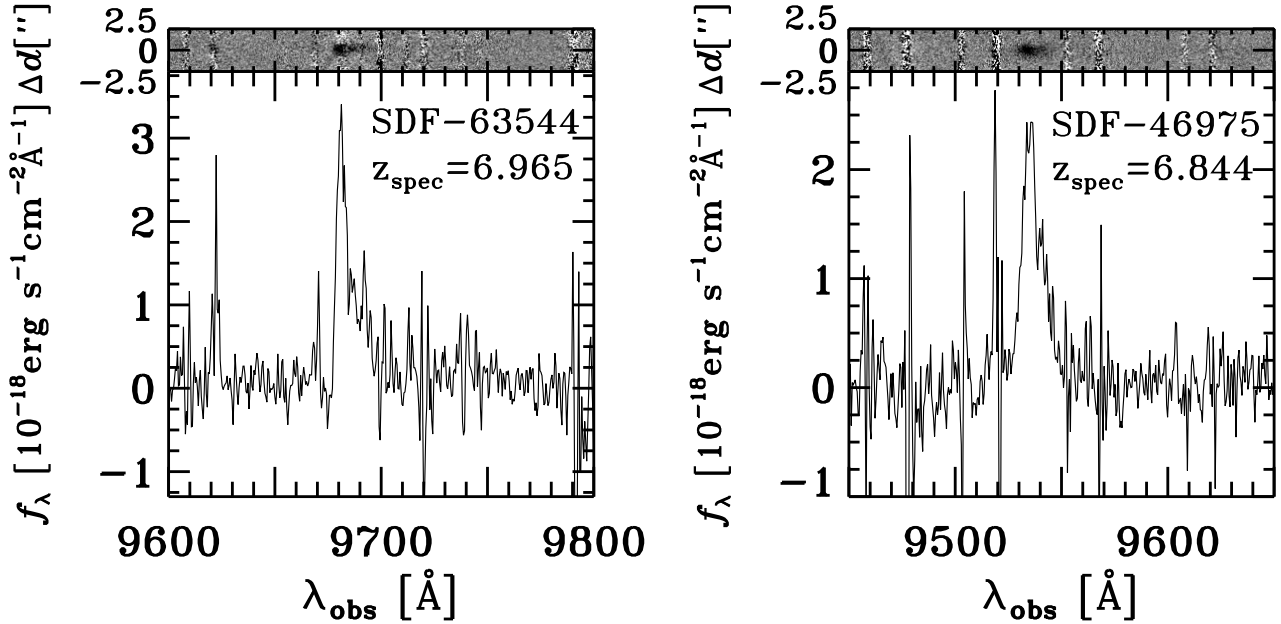


FIG. 1.— Spectra of SDF-63544 (left) and SDF-46975 (right). The top panels show the composite two-dimensional spectra, from which the one-dimensional spectra shown in the bottom panels are derived. A prominent emission line is seen at 9683 Å for SDF-63544 ($S/N \simeq 13$), and at 9536 Å for SDF-46975 ($S/N \simeq 14$).

observations of the z -dropout candidates discovered in Ouchi et al. (2009). The data were taken on UT 2010 February 13, April 14 – 15, and 2011 April 1 – 3. We observed 11 out of the 22 z -dropout candidates. We also observed the standard stars G191B2B and Wolf 1346 for flux calibration. The seeing was in the range $0.5'' - 0.7''$. We used a total of six DEIMOS masks, as listed in Table 1. For five masks, we used the OG550 filter and the 830 lines mm⁻¹ grating, which is blazed at 8640 Å and was tilted to place a central wavelength of 9000 Å on the detectors. This configuration provided a spectral coverage between 7000 Å and 10400 Å. For the remaining mask (HDF11C) we used the GG455 filter and the 600 lines mm⁻¹ grating, blazed at 7400 Å. This was tilted to place a central wavelength of 7500 Å on the detector. The spectral coverage was between 5200 Å and 10200 Å. The spatial pixel scale was $0.1185'' \text{ pix}^{-1}$, and the spectral dispersion was 0.47 Å pix^{-1} and 0.65 Å pix^{-1} for the 830 lines mm⁻¹ and 600 lines mm⁻¹ grating, respectively. The slit widths were $1''$. For objects filling the slit, the FWHM resolution of the 830 and 600 grating was $\simeq 3.3 \text{ Å}$ and $\simeq 4.7 \text{ Å}$, respectively¹⁴. Details of the

observations, the filters, gratings and the total exposure time used are listed in Table 1.

We used the GG455 filter for HDF11C, although this filter allows transmission of second-order light redward of $\sim 9100 \text{ Å}$. This filter was used because some of the targets on those masks were $z \sim 3$ ultra-luminous infrared galaxy candidates, which would have spectral signatures below 5000 Å. Although this configuration allowed contamination from second-order light of an emission line whose wavelength is longer than $\simeq 4500 \text{ Å}$, the targeted z -dropouts in the HDF11C mask were also observed in other configurations without such contaminations in the red wavelength range.

The reduction was performed using the `spec2d` IDL pipeline¹⁵ developed by the DEEP2 Redshift Survey Team (Davis et al. 2003). We used a modified version of the `spec2d` (Capak et al. in prep.) for the data taken with HDF11D, since those data were dithered. Wavelength calibration was achieved by fitting to the arc lamp emission lines. The spectra were flux calibrated with the standard stars G191B2B and Wolf 1346. We applied no

¹⁵ The pipeline was developed at UC Berkeley with support from NSF grant AST-0071048. Downloaded at <http://astro.berkeley.edu/~cooper/deep/spec2d/>

¹⁴ <http://www2.keck.hawaii.edu/inst/deimos/specs.html>

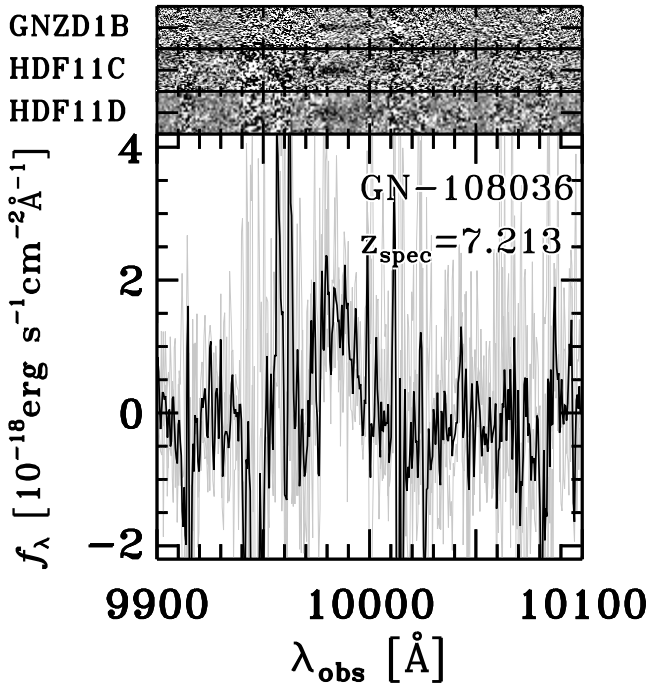


FIG. 2.— Spectrum of the $z = 7.213$ z -dropout galaxy, GN-108036. The top panels show its two-dimensional spectra obtained with the GNZD1B, HDF11C, and HDF11D masks. The size along the spatial axis is $5.0''$ for each two-dimensional spectrum. The HDF11D spectrum is binned in 2×2 pixels. A line is visually identified at $\simeq 9980\text{\AA}$ in the spectra of GNZD1B and HDF11C, whose exposure times are 5 hours and $\simeq 4$ hours, respectively, while the line is marginally seen in the spectrum of HDF11D, whose exposure time is 2 hours. In the bottom panel, we show the one-dimensional spectra. The gray solid lines are spectra obtained with individual masks. The composite spectrum is shown as the black solid line. All the one-dimensional spectra illustrate a line detection at around 9980\AA , and the S/N ratio of the line in the composite spectrum is $\simeq 6$.

correction for slit-loss effects, since the same slit width was used for both the standard stars and science targets. We estimate the uncertainty due to the slit-loss correction by comparing the fluxes of the two-dimensional spectra in the slit width with total fluxes and find this to be less than 10%. We measure the 1σ sky noises from the pixel distributions around 9600\AA , the wavelength corresponding to that of $\text{Ly}\alpha$ at $z \approx 6.9$, the expected peak of the redshift distribution for z -dropout selection (Figure 6 of Ouchi et al. 2009). In the measurements, we do not avoid the wavelength ranges significantly affected by strong OH lines. We find the 1σ sky noise to be $(1.4\text{--}5.7) \times 10^{-18}\text{ erg s}^{-1}\text{ cm}^{-2}$ (for details, see Section 4.2). We summarize the 1σ flux limits in Table 2.

4. RESULTS

4.1. Redshift Identification

Figure 1 shows a prominent emission line in the spectra of SDF-63544 and SDF-46975. We fit Gaussian profiles to these lines using the IDL MPFIT routine (Markwardt 2009)¹⁶, and find the emission lines correspond to the observed central wavelengths 9683\AA (SDF-63544) and 9536\AA (SDF-46975)¹⁷. One z -dropout galaxy, SDF-

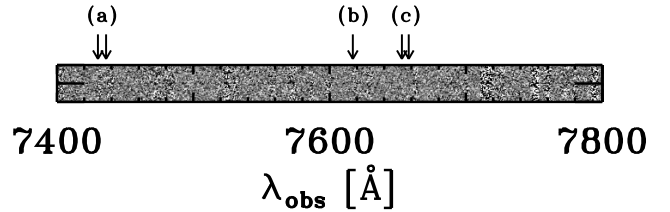


FIG. 3.— Two-dimensional spectrum of GN-108036 in the wavelength range of $7400 - 7800\text{\AA}$. The size along the spatial axis is $5.0''$. No emission line is detected in this wavelength range, which argue against the possibility that the detected line at $\simeq 9980\text{\AA}$ is $\text{H}\alpha$ at $z = 0.521$. In this case, an $[\text{OIII}]\lambda 5007$ line would have been detected at approximately 7617\AA marked by an arrow (b). No line detection also suggests that the detected line at $\simeq 9980\text{\AA}$ is not either an $[\text{OIII}]\lambda 5007$ at $z = 0.994$ or $\text{H}\beta$ at $z = 1.054$. In the former/latter case, the $[\text{OII}]\lambda\lambda 3726, 3729$ doublet would have been detected at the position marked by arrows (a)/(c).

63544, was previously identified as a $\text{Ly}\alpha$ emitter, IOK-1, whose redshift was confirmed spectroscopically by Iye et al. (2006). However, the signal-to-noise ratio (S/N) of the $\text{Ly}\alpha$ line in their spectrum is only $\simeq 5$. We deemed it worthwhile to detect the line at higher S/N and with higher resolution in order to verify the line detection and identify the line based on line profile analysis. We confirm that the central wavelength of the emission line is almost the same as that derived previously (9682\AA).

For one of the targets in GOODS-N, GN-108036, we detect an emission line at about 9980\AA (Figure 2). We confirm the line detection in three independent DEIMOS observations, performed in 2010 and 2011, with different configurations. In 2010, we obtained the spectrum using mask GNZD1B, the 830 lines mm^{-1} grating, and the OG550 filter (first two-dimensional spectrum in the top panel in Figure 2). In the 2011 run, we used a different set up with the 600 lines mm^{-1} grating, the GG455 filter, and a different mask (HDF11C) to locate the spectrum on a different position on the DEIMOS CCD (second one in the top panel in Figure 2). The HDF11D data were obtained over two nights of observing, and the line is detected in independent reductions of each night's data, as well as in the combined spectrum. We also used a third configuration for our 2011 run, with the 830 lines mm^{-1} grating, the OG550 filter, and an entirely new mask HDF11D (third one in the top panel in Figure 2). Although the grating and the filter here are the same as those used in the 2010 observation, the mask is different. The 2011 observations with the 830 grating were also dithered, whereas the 2010 observations with the 830 grating were undithered, and the pipeline processing was correspondingly different for the two data sets. The three observations of GN-108036 independently confirm that the line is detected at three different positions on the DEIMOS CCDs, with two different spectroscopic setups. This strongly argues against the observed feature being an artifact. We fit Gaussian functions to the line profile in Figure 2, using the MPFIT routine, and find a central wavelength of 9984\AA .

We investigate the possibility that the observed lines

¹⁶ <http://www.physics.wisc.edu/~craigm/idl/idl.html>

¹⁷ The best-fit central wavelengths are slightly shorter ($\sim 3\text{\AA}$), if we fit an asymmetric Gaussian profile in which the standard

deviation on the blue side is smaller than that on the red side, as a better approximation of the observed profiles but with an additional free parameter.

TABLE 2
SUMMARY OF FOLLOW-UP SPECTROSCOPY

Object	Mask	Total Exposure [sec]	flux limit (1σ) [erg s ⁻¹ cm ⁻²]	$y^{(\text{total})}$ [mag]	EW ₀ ^{Lyα} limit (3σ) [Å]
GN-152505	GNZD1B, HDF11C, HDF11D	39800	3.0×10^{-18}	25.2	10
GN-108036 [†]	GNZD1B, HDF11C, HDF11D	39800	4.2×10^{-18}	25.5	7.1
SDF-63544 [†]	SDFZD1B, SDFZD3	49350	2.1×10^{-18}	25.1	5.8
SDF-83878	SDFZD1B	19350	3.3×10^{-18}	25.1	12
SDF-46975 [†]	SDFZD1B, SDFZD3	49350	1.9×10^{-18}	25.2	7.1
SDF-76507	SDFZD1B	19350	2.4×10^{-18}	25.2	9.2
SDF-123919	SDFZD4	7200	5.3×10^{-18}	25.4	31
SDF-75298	SDFZD1B	19350	1.4×10^{-18}	25.5	6.5
SDF-121418	SDFZD4	7200	4.5×10^{-18}	25.6	31
SDF-107344	SDFZD4	7200	5.7×10^{-18}	25.7	53
SDF-136726	SDFZD4	7200	5.1×10^{-18}	25.7	45

NOTE. — The flux limits of the objects with Ly α detections (GN-108036, SDF-63544, and SDF-46975) were estimated using the sky-noise distribution in the vicinity of the Ly α line, while those of objects lacking Ly α detections were estimated using the sky-noise distribution between 9400 – 9800 Å. The EW₀^{Ly α} limits of the Ly α -detected objects were estimated by dividing their Ly α flux limits by their UV continuum flux densities and $(1 + z_{\text{spec}})$, while those of objects without Ly α detection were estimated assuming their redshifts are equal to 6.9.

[†] z -dropout with Ly α detection.

TABLE 3
PROPERTIES OF SPECTROSCOPICALLY CONFIRMED LY α -EMITTING z -DROPOUTS

Object	Redshift	$f^{\text{Ly}\alpha}$ [erg s ⁻¹ cm ⁻²]	$L^{\text{Ly}\alpha}$ [erg s ⁻¹]	m_{cont} [mag]	M_{cont} [mag]	EW ₀ ^{Lyα} [Å]	S_w [Å]	FWHM [Å]	V_{FWHM} [km s ⁻¹]
GN-108036	7.213	2.5×10^{-17}	1.5×10^{43}	25.2	-21.8	33	$4.1^{+0.7}_{-0.7}$	15	442
SDF-63544	6.965	2.8×10^{-17}	1.6×10^{43}	25.4	-21.6	43	$12.6^{+0.4}_{-0.4}$	6.7	207
SDF-46975	6.844	2.7×10^{-17}	1.5×10^{43}	25.4	-21.5	43	$8.6^{+0.6}_{-0.7}$	12	374

are something other than Ly α (i.e., H α , H β , [OII], or [OIII]). The main argument in favor of the observed lines being Ly α is their morphology and the clear asymmetry of the lines (see below). Furthermore, the lines are unlikely to be H β or [OIII] at $z \sim 0.9 - 1.0$, since, in this case, we expect to detect additional lines. If the detected line were H β , the [OIII] λ 5007 line would fall at 9972Å for SDF-63544, 9822Å for SDF-46975, and 10284Å for GN-108036. However, none of the objects show the corresponding detections, implying the line ratio [OIII] λ 5007/H β of $\lesssim 0.2 - 0.5$ (3σ upper limit). Galaxies with $12 + \log(\text{O}/\text{H}) \gtrsim 8.8 - 9.0$ meet these low ratios (e.g., Nagao et al. 2006), but our objects are unlikely to be such metal rich, because if they were, they should be very massive (from the mass-metallicity relation) and thus their broadband magnitudes would be much brighter than observed. In the case that the detected line were [OIII] λ 5007, the H β line would be seen at 9401Å for SDF-63544, 9259Å for SDF-46975, and 9674Å for GN-108036. However, none of the objects show the corresponding detections, implying the line ratio [OIII] λ 5007/H β of $\gtrsim 2.0 - 4.0$ (3σ lower limit). These lower limits correspond to subsolar oxygen abundances ($\sim 7.0 - 8.7$; See Figure 17 of Nagao et al. 2006), which may be typical of low-mass galaxies. Thus, unfortunately the non-detection of H β cannot strongly rule out the possibility of our objects being [OIII] λ 5007 emitters. In addition, the lines are unlikely to be [OII]. If the lines were [OII] emitters at $z \sim 1.6$, the FWHM resolution of 3.3Å would have distinguished the two compo-

nents of the doublet, separated by $\sim 7\text{Å}$. In their Figure 10, Hu et al. (2004) showed the spectra of emission-line objects with the [OII] doublet signature, which were obtained with Keck/DEIMOS using the same configuration as ours (the 830 grating and the OG550 filter). The fact that the detected lines in our spectra are singlet strongly argues against the possibility that they are $z \sim 1.6$ [OII] emitters. Moreover, the non-detection of the galaxies in the deep i -band images¹⁸ strongly disfavors the possibility that these galaxies are actually at $z \sim 1.6$. For GN-108036, if the detected line were H α at $z = 0.521$, then we might also expect to detect [OIII] or H β , which is actually not detected as shown in Figure 3. For SDF-63544 and SDF-46975, we cannot check the detection of [OIII] λ 5007 since their spectra do not cover the wavelength range blueward of 7500Å.

To quantify the asymmetry of the lines, we introduce the weighted skewness parameter, S_w , following Kashikawa et al. (2006). This can be used to distinguish Ly α from other emission lines. S_w is defined as the product of the skewness (the third moment of flux distribution) and the width of the line. Ly α emission lines at high redshifts typically have large positive S_w values, while other possible lines, H α , H β , and [OIII], are nearly symmetric and have almost zero values of S_w . When the [OII] line is not resolved, its S_w value is expected to be small, since the [OII] λ 3726 line is weaker than [OII] λ 3729 (e.g., Rhoads et al. 2003). The

¹⁸ The 2σ limiting total magnitude of the SDF (GOODS-N) i -band image is 28.3 (27.6).

S_w values of the three z -dropouts are estimated to be $S_w = 12.6 \pm 0.4 \text{ \AA}$ for SDF-63544, $S_w = 8.6^{+0.6}_{-0.7} \text{ \AA}$ for SDF-46975, and $S_w = 4.1 \pm 0.7 \text{ \AA}$ for GN-108036, which means that all the three lines have an asymmetric profile with a sharp decline on the blue side and a long tail on the red side, as is commonly seen in $\text{Ly}\alpha$ at high redshifts (e.g., Shimasaku et al. 2006; Kashikawa et al. 2006). Kashikawa et al. (2006) empirically set $S_w = 3 \text{ \AA}$ as a critical value to distinguish $\text{Ly}\alpha$ emission from other emission lines for galaxies at $z > 5.7$ (see also, Shimasaku et al. 2006). Our objects have higher S_w than the criterion, which would suggest that the detected lines are $\text{Ly}\alpha$.

Note that the asymmetric line profile in the spectra of GN-108036 might be caused by over-subtractions of OH lines blueward of the detected line. However, there is a window of OH lines near the detected line at the blue side. If the line had a symmetric profile, then we would expect to see faint emission in this window, similar to that seen on the red side of the line profile, but none is actually detected. The sky subtraction might affect the line profile to some extent, but the asymmetric line profile is likely to be real. In addition, there is no line detected other than the one at $\simeq 9980 \text{ \AA}$. Furthermore, the galaxy is not detected in the deep optical broadband images from either Subaru or HST/ACS. Its colors ($z - y > 1.6 (2\sigma)$, $y - m_{\text{F140W}} = 0.3$) are consistent with those expected for a LBG at $z = 7.2$. All of these factors support the interpretation that the detected line is redshifted $\text{Ly}\alpha$.

Thus, we conclude that all of the detected lines are redshifted $\text{Ly}\alpha$. The redshifts derived from the $\text{Ly}\alpha$ emission centroids are $z_{\text{spec}} = 6.965$ for SDF-63544, $z_{\text{spec}} = 6.844$ for SDF-46975, and $z_{\text{spec}} = 7.213$ for GN-108036. These redshifts might be overestimated since the $\text{Ly}\alpha$ emission lines of LBGs are typically shifted redward of their systemic redshifts (e.g., Pettini et al. 2001; Shapley et al. 2003; Steidel et al. 2010). The velocity offsets are typically less than $\sim 1000 \text{ km s}^{-1}$, which corresponds to a difference between the systemic redshift (z_{sys}) and that estimated from the $\text{Ly}\alpha$ line ($z_{\text{Ly}\alpha}$) of $\Delta z = z_{\text{sys}} - z_{\text{Ly}\alpha} \lesssim -0.027$.

$\text{NV } \lambda 1240$ is the only high-ionization metal line, indicative of AGN activity, which would fall within our spectral range. The line would fall at 9876 \AA for SDF-63544, 9727 \AA for SDF-46975, and 10184 \AA for GN-108036. None of the objects shows this emission line, placing a 3σ lower limit to the line ratio $\text{Ly}\alpha/\text{NV}$ of $\gtrsim 4$ for SDF-63544, $\gtrsim 5$ for SDF-46975, and $\gtrsim 2$ for GN-108036. However, since a typical high- z AGN has a line ratio of $\text{Ly}\alpha/\text{NV} = 4 - 20$ (e.g., McCarthy 1993), these lower limits are mostly not useful to exclude the possibility that the objects are AGN hosts; to do so much deeper spectroscopy is needed. Throughout this paper, we assume that the light of our objects is not contaminated by AGNs.

4.2. Line Flux Measurement

We compute the $\text{Ly}\alpha$ line flux by summing flux densities around the line, neglecting the minor contribution of UV continuum. This corresponds to the range $9677 - 9699 \text{ \AA}$ for SDF-63544, $9526 - 9551 \text{ \AA}$ for SDF-46975, and $9977 - 9997 \text{ \AA}$ for GN-108036. The estimated fluxes are summarized in Table 3.

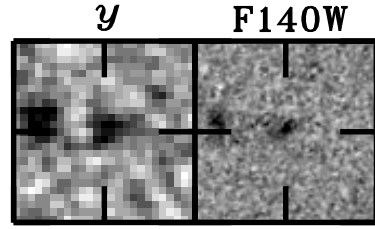


FIG. 4.— Images of GN-108036 taken by the Subaru Suprime-Cam (y), and HST WFC3 (F140W). The size of each panel is $5'' \times 5''$. North is up and east is to the left.

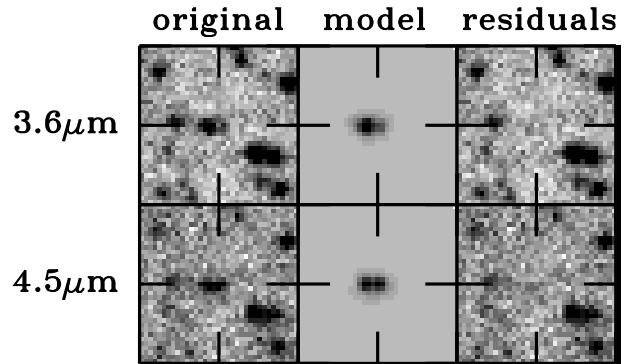


FIG. 5.— Images of GN-108036 in the IRAC $3.6\mu\text{m}$ (top) and $4.5\mu\text{m}$ (bottom). The panels from left to right show the original IRAC images, the best-fit model images constructed from PSF templates at the object positions measured from the HST WFC3 image, and the residuals after subtracting the model from the data. The size of each panel is $20.4'' \times 20.4''$. North is up and east is to the left.

SDF-63544 was previously discovered by Iye et al. (2006) who report $\text{Ly}\alpha$ fluxes of $2.0 \times 10^{-17} \text{ erg s}^{-1} \text{ cm}^{-2}$ and $2.7 \times 10^{-17} \text{ erg s}^{-1} \text{ cm}^{-2}$ from their spectrum and narrow-band image, respectively. Our estimated $\text{Ly}\alpha$ flux of SDF-63544 is $2.8 \times 10^{-17} \text{ erg s}^{-1} \text{ cm}^{-2}$, consistent with those previous measurements.

In order to estimate flux limits for the objects without $\text{Ly}\alpha$ detections, for each object we sample the one-dimensional spectra in 25 \AA bins, comparable to the width of $\text{Ly}\alpha$ lines. We then estimate the 1σ flux limit by fitting Gaussian functions to the flux distribution over the wavelength range $9400 - 9800 \text{ \AA}$. The 1σ flux limits for individual objects are listed in Table 2.

4.3. Equivalent Width Measurement

We do not directly detect continuum in the spectra of the z -dropout galaxies. We can only estimate their continuum flux densities from their y -band magnitudes measured over a 1.8 arcsec diameter aperture (Table 3 of Ouchi et al. 2009), allowing for aperture corrections, IGM absorption and $\text{Ly}\alpha$ emission.

To estimate the aperture correction for our z -dropouts, we select bright, non-saturated and isolated sources in the y -band images, and perform multi-aperture photometry to construct the curve of growth. We then determine the aperture correction by measuring the difference between magnitude over the 1.8 arcsec diameter aperture and the total magnitude (the asymptote of the growth curve). The median aperture correction is 0.344 mag for GOODS-N and 0.349 mag for the SDF.

TABLE 4
SED FITTING RESULTS FOR $z = 7.213$ GALAXY

model	Z [Z_{\odot}]	$\log M_{\text{star}}$ [M_{\odot}]	$E(B - V)_{\star}$ [mag]	$\log(\text{Age})$ [yr]	$\log(\text{SFR})$ [$M_{\odot} \text{ yr}^{-1}$]	$\log(\text{SSFR})$ [yr^{-1}]	χ^2
stellar + nebular	0.2	$8.76^{+0.10}_{-0.12}$	$0.05^{+0.02}_{-0.03}$	$6.76^{+0.10}_{-0.12}$	$2.00^{+0.02}_{-0.01}$	$-6.76^{+0.14}_{-0.17}$	12.8
pure stellar	0.2	$9.35^{+0.12}_{-0.11}$	$0.11^{+0.01}_{-0.01}$	$7.38^{+0.13}_{-0.12}$	$2.00^{+0.02}_{-0.02}$	$-7.35^{+0.23}_{-0.20}$	23.8

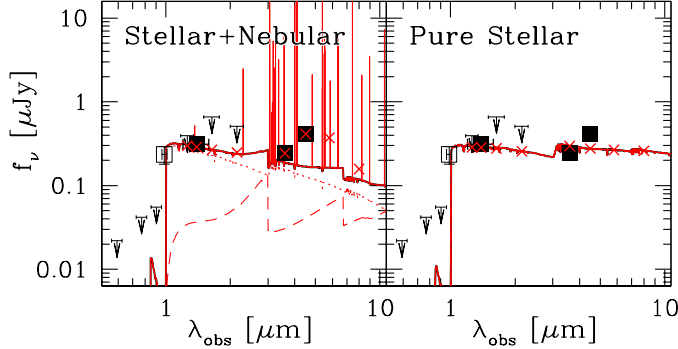


FIG. 6.— Results of SED fitting for the $z = 7.213$ galaxy GN-108036. The filled squares show the observed flux densities used for SED fitting, while the open squares show those not used. The vertical arrows show 5σ upper limits for HST/ACS V_{606} , i_{775} , z_{850} (Ouchi et al. 2009), Subaru/MOIRCS J , H , and K from left to right. The left panel is for ‘stellar + nebular’ ($f_{\text{esc}}^{\text{ion}} = 0$) models. The red solid curve indicate the best-fit SED that is the sum of a stellar SED (red dotted curve) and a nebular SED (red dashed curve). The crosses indicate synthesized flux densities in individual bandpasses. The right panel is for ‘pure stellar’ ($f_{\text{esc}}^{\text{ion}} = 1$) models.

The flux in the y -band is affected by Ly α emission and IGM absorption shortward of rest-frame 1216Å. We correct for the contribution due to Ly α emission using the estimated Ly α flux from section 4.2 for objects with strong Ly α emission, and the 3σ flux limit for the z -dropouts without Ly α detection. The IGM absorption is taken into account on the assumption of flat UV continuum in f_{ν} and using Madau (1995). The 3σ EW limits for the 11 galaxies in the spectroscopic sample are listed in Table 2. In Table 3, we list our estimates for the continuum magnitude m_{cont} at the Ly α wavelength, and the corresponding EWs that we derived for the Ly α emission lines.

4.4. Photometry and Stellar Population Properties of the $z = 7.213$ galaxy

The Subaru y -band photometry for the $z = 7.2$ galaxy GN-108036 is difficult to interpret because the flux measurement is strongly affected both by the Ly α emission line and the Ly α forest IGM absorption, which should suppresses roughly 65% of the intrinsic continuum flux from the galaxy within the y bandpass. Fortunately, GN-108036 has been imaged with the HST WFC3-IR camera (Weiner et al. in preparation; HST program #11600). The image has a total exposure time of 1217 sec and was obtained with the F140W filter, whose central wavelength is approximately $1.4\mu\text{m}$, sampling 1700Å in the rest-frame UV continuum. The Suprime-Cam y -band and WFC3 F140W images of GN-108036 are shown in Figure 6. Photometry in the HST image measures a total magnitude of 25.17 ± 0.07 mag. GN-108036 was also observed in the Subaru MOIRCS JHK survey of the GOODS-N field (Kajisawa et al. 2011). The galaxy is

not significantly detect in any of these MOIRCS bands, with 5σ photometric upper limits of 24.9 (J), 24.4 (H), and 24.6 (K), marginally consistent with the WFC3 photometry.

The WFC3 F140W magnitude of GN-108036, $m = 25.17$, translates to a rest-frame 1700Å luminosity $M_{1700} = -21.81$ at $z = 7.213$. There have been many recent estimates of the UV luminosity function at $z = 7$ (e.g., Ouchi et al. 2009; Oesch et al. 2010; McLure et al. 2010; Grazian et al. 2011). These have consistently found values of the characteristic luminosity M^* in the range -19.9 to -20.3 . GN-108036 is therefore an impressively luminous galaxy, with $L_{\text{UV}} \approx 4$ to $6L^*$; indeed, it is roughly twice as bright as an L_{UV}^* LBG at $z = 2$ to 3 ($M_{\text{UV}}^* \approx -21.0$, Reddy et al. 2008). The exponential cut-off of a Schechter luminosity function would imply that galaxies this luminous would be rare indeed. For example, the best-fit Schechter parameterization of the $z = 7$ luminosity function from Bouwens et al. (2011b) yields a space density $2.7 \times 10^{-7} \text{ Mpc}^{-3}$ for galaxies with $M_{\text{UV}} \leq -21.81$. For a redshift interval $\Delta z = 1$ at $z = 7$, we would expect to find only 0.1 galaxies this luminous within the 160 arcmin² GOODS-N ACS/WFC3/IRAC field, or about 1 galaxy over the 1568 arcmin² covered by our Suprime-Cam survey in the combined SDF and GOODS-N fields. In fact, the redshift selection function for z -dropouts in our z - y survey is significantly narrower than $\Delta z = 1$ (see Ouchi et al. 2009), making the large UV luminosity of GN-108036 still more remarkable. It is impossible to judge based on *a posteriori* statistics from a single object, but either we were quite lucky to find and spectroscopically confirm such a bright galaxy, or perhaps the bright end of the UV luminosity function at $z = 7$ has been underestimated in studies to date. In fact, the observational constraints on the bright end of the luminosity function come from just a few ground-based surveys, including our own (Ouchi et al. 2009) and that of Castellano et al. (2010a,b). Evidently more deep imaging and spectroscopic studies over wider fields are needed to provide better measurements. The y -band itself becomes an unreliable indicator of luminosity for galaxies at $z > 7$ without exact measurements of the galaxy redshift and Ly α line flux, so deep near-infrared data at longer wavelengths (such as that from HST WFC3) will be essential for a robust determination of the luminosity function.

GN-108036 also falls within the field covered by the extremely deep IRAC imaging from the GOODS Spitzer Legacy program (PI: M. Dickinson). As was noted in Ouchi et al. (2009), the galaxy is faintly detected in the IRAC 3.6 μm and 4.5 μm images, which roughly sample the rest-frame B and V band light at $z = 7.2$, although it is partially blended with a foreground galaxy located $1''$ to the east (Figure 5). In order to extract reliable IRAC fluxes, we measure the positions of the two galax-

ies in the WFC3 F140W image, and then position unit-normalized IRAC PSF images at these locations in the background-subtracted $3.6\mu\text{m}$ and $4.5\mu\text{m}$ images. We then fit these PSF templates to the IRAC data, minimizing χ^2 to derive the best-fitting fluxes and their uncertainties. The middle panels in Figure 5 show the best-fit model and the right panels are the residual images. In this way, we obtain the total magnitudes of GN-108036 of $m_{3.6\mu\text{m}} = 25.44 \pm 0.13$ and $m_{4.5\mu\text{m}} = 24.86 \pm 0.13$, respectively.

We fit models to the photometry of GN-108036 to infer its stellar population properties. The procedure is the same as that of Ono et al. (2010), except that redshift is fixed at $z = 7.213$. We use the stellar population synthesis model GALAXEV (Bruzual & Charlot 2003) for the stellar component of the SEDs, and consider two extreme cases for nebular emission: $f_{\text{esc}}^{\text{ion}} = 0$, where ionizing photons are all converted into nebular emission (the ‘stellar + nebular’ case), and $f_{\text{esc}}^{\text{ion}} = 1$, where all ionizing photons escape from the galaxy (the ‘pure stellar’ case). Nebular spectra (lines and continua) are calculated following the procedure given in Schaerer & de Barros (2009). We adopt the Salpeter initial mass function (IMF; Salpeter 1955), a constant rate of star formation, and stellar and gas metallicities $Z = 0.2Z_{\odot}$. For dust attenuation, we use the functional form of Calzetti et al. (2000) with the assumption that $E(B - V)_{\text{gas}} = E(B - V)_{\star}$, as proposed by Erb et al. (2006). The model SEDs are fit to the observed flux densities in the WFC3 F140W and IRAC $3.6\mu\text{m}$ and $4.5\mu\text{m}$ bands, and its MOIRCS JHK magnitudes. We do not use the y -band photometry since it is strongly affected by IGM attenuation and $\text{Ly}\alpha$ emission. The free parameters in the fitting are stellar mass, age, and dust extinction, with three degrees of freedom.

The results of SED fitting are summarized in Table 4, and the best-fitting SEDs are shown in Figure 6. The best-fit models have small stellar masses, $4 \times 10^8 M_{\odot}$ to $3 \times 10^9 M_{\odot}$, very young ages, 4 to 32 Myr, and modest color excesses $E(B - V)_{\star} = 0.02$ to 0.12 ¹⁹. Deeper K -band photometry would be needed to reliably constrain the amplitude of the Balmer break, but the blue rest-frame UV-to-optical color $m_{\text{F140W}} - m_{3.6\mu\text{m}} = -0.27$ suggests that the break is small and that the light from the galaxy is dominated by very young and relatively unreddened stars.

If the flux in the IRAC bands has a significant contribution from nebular emission, then the intrinsic stellar SED would be even bluer than the directly measured WFC3-to-IRAC color would suggest (see Figure 6, left). There is evidence that this is the case. The very red IRAC $3.6\mu\text{m}$ to $4.5\mu\text{m}$ color is not easily reproduced by stellar emission alone, but can be explained by a strong contribution of nebular emission in the $4.5\mu\text{m}$ bandpass. At $z = 7.2$, the IRAC $3.6\mu\text{m}$ band is mostly free of strong emission lines, but the IRAC $4.5\mu\text{m}$ band includes $[\text{OIII}]\lambda 4959$ and $\lambda 5007$ ($\text{H}\beta$ is largely excluded). Several recent studies have suggested that strong nebular emission lines can significantly affect IRAC photometry for high redshift galaxies (e.g., Schaerer & de Barros 2009; Vanzella et al. 2010; Raiter et al. 2010; Ono et al. 2010;

Shim et al. 2011), and galaxies with extremely strong $[\text{OIII}]$ ($\text{EW}_0 > 1000\text{\AA}$) have been identified at $z < 1$ (e.g., Kakazu et al. 2007) and $z = 1$ to 1.5 (Atek et al. 2010). Here we see evidence for strong $[\text{OIII}]$ at $z = 7.2$; in the best-fit stellar+nebular model, the $[\text{OIII}]$ lines contribute $\sim 60\%$ of the flux in the IRAC $4.5\mu\text{m}$ band.

Using the conversion from UV continuum luminosity density to star formation rate from Madau et al. (1998) for a Salpeter IMF, and assuming no extinction, the 1700\AA luminosity of GN-108036 implies a star formation rate (SFR) of $29M_{\odot} \text{ yr}^{-1}$. However, the best-fitting stellar population models give larger SFR $\approx 100M_{\odot} \text{ yr}^{-1}$ (Table 4). In part this is due to extinction in the models, and in part to the very young ages that are implied by the SED-fitting. The standard conversion factors of UV luminosity per unit SFR (e.g., from Madau et al. 1998, or Kennicutt 1998) assume star formation timescales $\gtrsim 10^8$ years. At younger ages, the UV continuum is still building toward its steady-state value, and SFRs derived using the standard conversion factors will be underestimated. For comparison, the $\text{Ly}\alpha$ line luminosity ($1.5 \times 10^{43} \text{ erg s}^{-1}$) yields another estimate of $\text{SFR}(\text{Ly}\alpha) = 13.6M_{\odot} \text{ yr}^{-1}$, again adopting a standard Salpeter IMF conversion factor (Kennicutt 1998) and assuming Case B recombination for the $\text{H}\alpha/\text{Ly}\alpha$ flux ratio. This SFR is significantly smaller than either estimate from the continuum SED, as expected since $\text{Ly}\alpha$ is subject to strong attenuation from dust extinction and by the IGM.

Because the unusual IRAC color of GN-108036 strongly favors the results from the ‘stellar+nebular’ model fitting, we conclude that the stellar mass of this galaxy is most likely smaller than $10^9 M_{\odot}$. This value is not atypical compared to other published estimates for galaxies at $z \sim 7$ (e.g., Finkelstein et al. 2010; González et al. 2011). However, when combined with the bright UV luminosity and the large derived star formation rate, it implies an extremely high specific star formation rate ($\text{SSFR}) > 10^{-7} \text{ yr}^{-1}$. This is at least 50 times higher than the mean values that have been estimated for samples of LBGs at $4 < z < 7$ (González et al. 2010), and suggests that GN-108036 is seen at a special moment in its life cycle when it is undergoing a very strong starburst, presumably with a short duration.

Although the IRAC color favors ‘stellar+nebular’ modeling, the very young age derived may be in conflict with a simple expectation that the duration of star formation cannot be shorter than the dynamical time of the system, since it will take around the dynamical time to have the gas of the system collapse to form stars. GN-108036 has an FWHM of $0.30''$ in the F140W image and a $\text{Ly}\alpha$ line width of $4.4 \times 10^2 \text{ km s}^{-1}$. Dividing the former by the latter gives a rough estimate of the dynamical time of ~ 4 Myr, which is marginally consistent with the age from SED fitting. Although this possible problem is not directly related to the discussion and conclusions of this paper, similar conflicts between stellar age and dynamical time are found in other papers (e.g., Schaerer & de Barros 2009, 2010; Ono et al. 2010), highlighting the need for further research.

Assuming a flat f_{ν} UV spectral slope, we derive an equivalent width for $\text{Ly}\alpha$ $\text{EW}_0^{\text{Ly}\alpha} = 33\text{\AA}$. Another galaxy from our sample, SDF-63544, was also observed with HST/WFC3 in the F125W, F140N, and F160W band-

¹⁹ The uncertainties should be larger if star-formation history and metallicity are varied, although we fix them due to the small number of the data points.

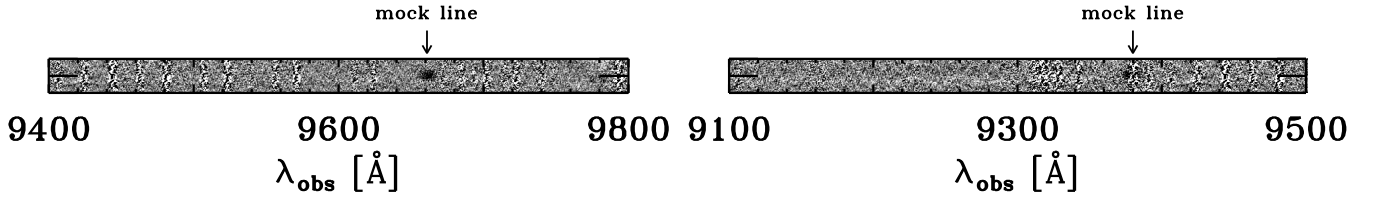


FIG. 7.— Examples of mock spectra made by artificially adding a mock emission line to the two-dimensional spectrum of GN-152505. The mock emission line has Ly α equivalent width of 50 \AA and continuum magnitude of 25.57. The left panel shows a spectrum whose mock line is found at $\simeq 9660\text{\AA}$, while a mock line ($\simeq 9380\text{\AA}$) is not recovered in the right spectrum due to the residuals of severe OH lines around the artificial line.

passes (Cai et al. 2011, Egami et al. in preparation). A fit to this photometry yields a UV continuum slope $f_{\lambda} \propto \lambda^{-2.46}$ (Cai et al. 2011), and a continuum flux magnitude of 25.5 ± 0.1 at 9683 \AA , the wavelength of Ly α , consistent with our estimate from the y -band photometry in Section 4.3.

4.5. Ly α Fraction

In order to infer the ionizing state of the IGM, we study the evolution of the Ly α fraction by measuring its value at $z \sim 7$ and comparing it with previous measurements at $4 < z < 6$. For $4 < z < 6$ dropout galaxies, Stark et al. (2011) divided their sample into two UV luminosity bins, $-21.75 < M_{\text{UV}} < -20.25$ and $-20.25 < M_{\text{UV}} < -18.75$, and estimated their Ly α fractions. Since the UV absolute magnitudes of our z -dropouts are in the brighter range, in the following analysis for our sample we focus only on the Ly α fraction of dropout galaxies at $-21.75 < M_{\text{UV}} < -20.25$.

We define the Ly α fraction as the ratio of the number of z -dropout galaxies with strong Ly α emission measured from their spectra to the total number of spectroscopically observed z -dropouts,

$$X_{\text{Ly}\alpha}^{\text{EW}_c} = \frac{\sum_i \alpha_i^{\text{Ly}\alpha} p_i}{\sum_i p_i}, \quad (1)$$

where $\alpha_i^{\text{Ly}\alpha}$ is 1 if any i -th galaxy has a Ly α EW larger than a critical EW (EW_c) and 0 otherwise. p_i is the probability that the Ly α wavelength of the i -th z -dropout candidate is within the observable wavelength range - i.e., the range not contaminated by OH airglow lines, and is given by $p_i = \int C'_i(z) dz / \int C(z) dz$, where $C(z)$ is the probability distribution for z -dropouts as a function of redshift and $C'_i(z)$ is the effective redshift probability distribution function of z -dropout candidates when corrected for OH emission. Such a statistical analysis of the p_i parameter is needed since, at the wavelength range $\sim 9000 - 10100 \text{\AA}$, where we expect to detect their Ly α line, our $z \sim 7$ candidates may not always satisfy the EW_c criterion (i.e., $p_i = 1$), as the atmospheric OH airglow lines will significantly affect the spectrum in that wavelength range.

In order to compute $C'(z)$, we perform Monte Carlo simulations by generating mock Ly α emission lines with $\text{EW}_0 = 50\text{\AA}$ or 100\AA and y -band magnitudes of 25.24 and 25.57 mag. These magnitudes correspond to the central values of two bins into which the y -band total magnitudes of our z -dropouts are divided in order of their brightness. We add the mock Ly α lines to an observed two-dimensional spectrum, following the redshift distribution, $C(z)$ (Figure 6 in Ouchi et al. 2009). We then inspect the mock two-dimensional spectrum search-

ing for a Ly α feature. Figure 7 shows examples of two-dimensional spectra apparently with and without Ly α detected (left and right plots, respectively). We perform a number of trials and evaluate the recovery rate of mock Ly α lines. The $C'(z)$ is then estimated by computing the weighted mean of Ly α EWs, assuming this to be a Gaussian function (Ouchi et al. 2008). We find that over 90% of the mock Ly α lines are successfully recovered in our extremely deep spectra (i.e., $C'_i(z) \simeq C(z)$). Therefore, we choose not to correct for this effect in the following analysis. When computing the Ly α emission fraction, $X_{\text{Ly}\alpha}^{\text{EW}_c}$ above a certain equivalent width threshold EW_c , we divide the number of galaxies with *detected* $\text{EW}(\text{Ly}\alpha) > \text{EW}_c$ by the number of galaxies for which the 3σ upper limits to the EW detectability are smaller than EW_c (i.e., those galaxies for which Ly α lines stronger than EW_c could have been detected).

From the sample of 11 z -dropout galaxies with spectroscopic data studied here, we detect Ly α emission lines for 3 sources, all with Ly α EWs larger than 25 \AA . However, we do not include GN-108036 at $z = 7.2$, since it is brighter than -21.75 in the rest-frame UV. We find 4 objects with Ly α EW limits larger than this, giving a Ly α fraction, $X_{\text{Ly}\alpha}^{25} = 33 \pm 27\%$ (2/6). If we set the $\text{EW}_c = 55\text{\AA}$, the 2 objects with Ly α detection have smaller $\text{EW}_0^{\text{Ly}\alpha}$ than the criterion. The Ly α EW upper limits of 8 z -dropout candidates without Ly α detection are lower than the EW_c . We thus obtain an upper limit of Ly α fraction: $X_{\text{Ly}\alpha}^{55} < 10\%$ (0/10).

5. DISCUSSION: IMPLICATIONS FOR REIONIZATION

Since neutral hydrogen in the IGM resonantly scatters Ly α photons, the transmission of Ly α photons is sensitive to the ionization state of the IGM. Thus, the fraction of Ly α -emitting LBGs can be used as a diagnostic for the ionization state of the IGM. In Section 4.5, we estimated the Ly α fraction of bright z -dropout galaxies to be $X_{\text{Ly}\alpha}^{25} = 33 \pm 27\%$ (2/6), and $X_{\text{Ly}\alpha}^{55} < 10\%$ (0/10). In order to study evolution of the Ly α fraction to $z \sim 7$, we compare our estimates for the bright ($-21.75 < M_{\text{UV}} < -20.25$, or $M_{\text{UV}} \simeq -21$) z -dropout galaxies with those at $z \sim (4, 5, 6)$, $X_{\text{Ly}\alpha}^{25} = (12 \pm 3\%, 24 \pm 5\%, 20 \pm 8\%)$ and $X_{\text{Ly}\alpha}^{55} = (5.5 \pm 1.8\%, 7.2 \pm 2.8\%, 7.5 \pm 5.0\%)$ and their extrapolations to $z \sim 7$, $X_{\text{Ly}\alpha}^{25} = 33 \pm 10\%$ and $X_{\text{Ly}\alpha}^{55} = 9 \pm 6\%$, which are derived on the assumption of a linear relationship between Ly α fraction and redshift (Stark et al. 2011). For faint ($-20.25 < M_{\text{UV}} < -18.75$, or $M_{\text{UV}} \simeq -19.5$) galaxies at $z \sim (4, 5, 6)$, Stark et al. (2011) obtained their Ly α fractions of $X_{\text{Ly}\alpha}^{25} = (35 \pm 5\%, 48 \pm 9\%, 54 \pm 11\%)$ and

TABLE 5
 PROPERTIES OF z -DROPOUTS SPECTROSCOPICALLY OBSERVED IN THE PREVIOUS STUDIES

Object	Redshift ^a	m_{cont} ^b [mag]	M_{UV} ^c [mag]	$f^{\text{Ly}\alpha}$ ^d [$\text{erg s}^{-1} \text{cm}^{-2}$]	$\text{EW}_0^{\text{Ly}\alpha}$ [Å]	comments
Fontana et al. (2010)						
G2_1408	6.972	26.37	-20.49	3.4×10^{-18}	13	$S/N(\text{Ly}\alpha) = 7$, Castellano et al. (2010a), Y_{OPEN} Hawk-I
G2_2370	6.8	25.56	-21.27	$< 2.5 \times 10^{-18}$	< 4.8	Castellano et al. (2010a), Y_{OPEN} Hawk-I
G2_4034	6.8	26.35	-20.50	$< 2.5 \times 10^{-18}$	< 9.7	Castellano et al. (2010a), Y_{OPEN} Hawk-I
G2_6173	6.8	26.53	-20.33	$< 2.5 \times 10^{-18}$	< 11	Castellano et al. (2010a), Y_{OPEN} Hawk-I
H_9136	6.8	25.90	-20.94	$< 2.5 \times 10^{-18}$	< 6.4	Hickey et al. (2010), Y_{OPEN} Hawk-I
W_6	6.8	26.93	-20.38	$< 2.5 \times 10^{-18}$	< 11	Wilkins et al. (2010), Y_{098} WFC3-ERS
O_5	6.8	27.52	-19.67	$< 2.5 \times 10^{-18}$	< 21	Oesch et al. (2010), Y_{105} WFC3-HUDF
Vanzella et al. (2011)						
BDF-521	7.008	25.86	-20.63	1.62×10^{-17}	64	$S/N(\text{Ly}\alpha) = 18$
BDF-3299	7.109	26.15	-20.56	1.21×10^{-17}	50	$S/N(\text{Ly}\alpha) = 16$
Schenker et al. (2011)						
ERS5847	6.48 [†]	26.6	-20.22	—	—	—
ERS7376	6.79 [†]	27.0	-19.89	—	—	—
ERS7412	6.38 [†]	27.0	-19.79	—	—	—
ERS8119	6.78 [†]	27.1	-19.79	—	—	—
ERS8290	6.52 [†]	27.1	-19.73	—	—	with a close neighbor
ERS8496	6.441	27.3	-19.51	9.1×10^{-18}	65	$S/N(\text{Ly}\alpha) > 5$
ERS10270	7.02 [†]	27.4	-19.54	—	—	—
ERS10373	6.44 [†]	27.4	-19.41	—	—	—
A1703_zD1	6.75 [†]	24.1	-20.39	—	—	Magnification factor $\mu = 9.0^{\ddagger}$
A1703_zD3	6.89 [†]	25.5	-19.25	—	—	Magnification factor $\mu = 7.3^{\ddagger}$
A1703_zD6	7.045	25.8	-19.36	2.8×10^{-17}	65	Magnification factor $\mu = 5.2^{\ddagger}$, $S/N(\text{Ly}\alpha) > 5$
A1703_zD7	8.80 [†]	26.8	-18.74	—	—	Magnification factor $\mu = 5.0^{\ddagger}$
A2261_1	7.81 [†]	26.9	-18.85	—	—	Magnification factor $\mu = 3.5$
BoRG_4	8.27 [†]	25.8	-21.39	—	—	—
EGS_K1	8.27 [†]	25.3	-21.89	—	—	—
HUDF09_799	6.88 [†]	27.7	-19.21	—	—	—
HUDF09_1584	7.17 [†]	26.7	-20.27	—	—	—
HUDF09_1596	6.905	26.8	-20.12	—	30	—
MS0451-03_10	7.50 [†]	26.7	-16.10	—	—	Magnification factor $\mu = 50$
Pentericci et al. (2011)						
NTTDF-474	6.623	26.50	-20.35	3.2×10^{-18}	16	$S/N(\text{Ly}\alpha) = 7$
NTTDF-1479	6.8	26.12	-20.77	—	—*	—
NTTDF-1632	6.8	26.44	-20.45	—	—*	—
NTTDF-1917	—	26.32	—	—	—*	likely an interloper
NTTDF-2916	6.8	26.64	-20.25	—	—*	—
NTTDF-6345	6.701	25.46	-21.41	7.2×10^{-18}	15	$S/N(\text{Ly}\alpha) = 11$
NTTDF-6543	6.8	25.75	-21.14	—	—*	—
BDF4-2687	6.8	26.15	-20.74	—	—*	—
BDF4-2883	6.8	26.15	-20.74	—	—*	—
BDF4-5583	6.8	26.65	-20.24	—	—*	—
BDF4-5665	6.8	26.64	-20.25	—	—*	—

NOTE. — The upper limits of $\text{Ly}\alpha$ flux and equivalent width are 5σ .

^a The redshift of objects without spec- z is set at 6.8.

^b For the objects of Fontana et al. (2010), Vanzella et al. (2011), and Pentericci et al. (2011), Y -band magnitudes are taken from their Table 1, respectively. For the objects of Schenker et al. (2011), J_{125} magnitudes are taken from their Table 1.

^c Objects from Fontana et al. (2010) are taken from their Table 1. For the objects of Vanzella et al. (2011), it is calculated from the Y -band magnitude corrected for $\text{Ly}\alpha$ contribution and IGM attenuation, Y_{cont} . For the objects of Schenker et al. (2011) and Pentericci et al. (2011), it is calculated from the continuum magnitude m_{cont} and redshift. The magnification factors are considered for the Schenker et al. (2011) objects.

^d For the objects of Fontana et al. (2010), the upper limit is estimated from the 1σ limiting flux at 9485\AA , corresponding to $z \sim 6.8$ $\text{Ly}\alpha$, around which the redshift distribution of their z -dropouts peaks (Figure 1 in Castellano et al. 2010a).

[†] The photometric redshift estimated by Schenker et al. (2011) or McLure et al. (2011).

[‡] These are estimated by Bradley et al. (2011).

* The EW detection limits are well below $\text{EW} = 25\text{\AA}$ (Pentericci et al. 2011).

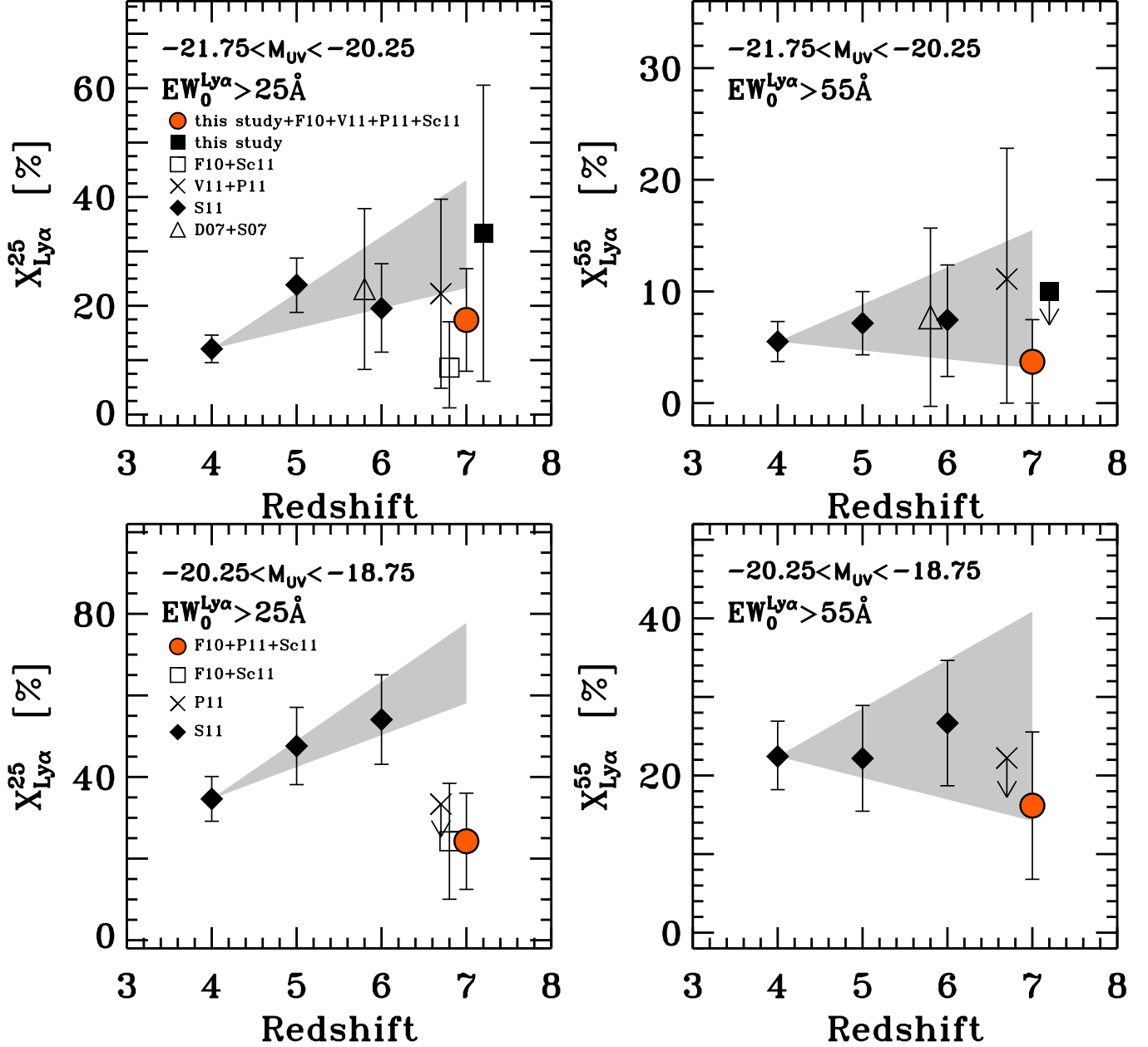


FIG. 8.— Evolution in the fraction of strong LAEs in LBGs with $-21.75 < M_{UV} < -20.25$ (top panels) and $-20.25 < M_{UV} < -18.75$ (bottom panels) over $4 < z < 7$. The left panels show the fraction of galaxies with EW larger than 25 \AA , while the right panels show the fraction of those with EW larger than 55 \AA . The filled square is our results, the open square is the results of Fontana et al. (2010) and Schenker et al. (2011), the cross is from Vanzella et al. (2011) and Pentericci et al. (2011), and the filled circle is the composite results. The filled diamonds are the results of Stark et al. (2011), and open triangle is the composite result of Dow-Hygelund et al. (2007) and Stanway et al. (2007). The filled square, open square, cross, and open triangle are shifted in redshift for clarity. The shaded area is derived by extrapolating the trend seen in lower redshifts to $z \sim 7$ (Stark et al. 2011).

TABLE 6
SUMMARY OF THE SAMPLES

	$EW_0^{Ly\alpha} > 25\text{\AA}$	$EW_0^{Ly\alpha} > 55\text{\AA}$
$-21.75 < M_{UV} < -20.25$		
This Study	2/6 [†]	0/10
Fontana et al. (2010)	0/6	0/6
Vanzella et al. (2011)	2/2	1/2
Schenker et al. (2011)	0/2	0/2
Pentericci et al. (2011)	0/7	0/7
$-20.25 < M_{UV} < -18.75$		
Fontana et al. (2010)	0/1	0/1
Schenker et al. (2011)	3/12	2/12
Pentericci et al. (2011)	0/3	0/3

NOTE. — For the sample of Schenker et al. (2011), objects at $6.3 < z < 7.3$ are considered.

[†] In our sample, four objects have Ly α EW limits larger than 25 \AA .

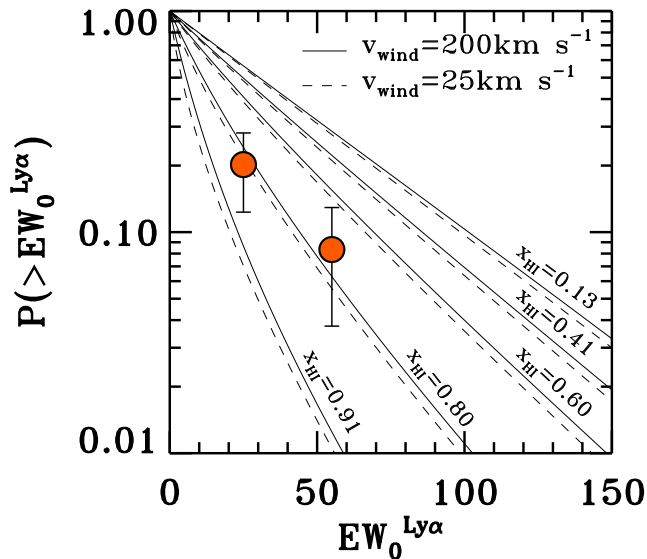


FIG. 9.— Cumulative distribution function (CDF) of rest-frame Ly α EW for $z \sim 7$ galaxies. The filled circles are the composite results. The solid lines show the $z = 7$ CDF for the wind model of Dijkstra et al. (2011) with column density $N_{\text{HI}} = 10^{20} \text{ cm}^{-2}$, wind velocity $v_{\text{wind}} = 200 \text{ km s}^{-1}$, and neutral hydrogen fraction x_{HI} of 0.13, 0.41, 0.60, 0.80, 0.91 from top to bottom. The dashed lines are the same as the solid lines, except that $v_{\text{wind}} = 25 \text{ km s}^{-1}$.

$X_{\text{Ly}\alpha}^{55} = (22 \pm 4\%, 22 \pm 7\%, 27 \pm 8\%)$ and their extrapolations to $z \sim 7$, $X_{\text{Ly}\alpha}^{25} = 67 \pm 10\%$ and $X_{\text{Ly}\alpha}^{55} = 27 \pm 13\%$.

For an independent check on the values from Stark et al. (2011), we refer to Dow-Hygelund et al. (2007) and Stanway et al. (2007), who presented the results of spectroscopy for i -dropout galaxies at $z \sim 6$. Dow-Hygelund et al. (2007) reported a total of 12 LBGs with bright UV continuum ($-21.75 < M_{\text{UV}} < -20.25$)²⁰. Three (one) of these galaxies are found to have Ly α EWs larger than 25 \AA (55 \AA). In an independent study, Stanway et al. (2007) found one such bright galaxy (ID 1042) with Ly α EW of 23 \AA . Combining these results, we estimate a Ly α fraction of $X_{\text{Ly}\alpha}^{25} = 23 \pm 15\%$ (3/13)

²⁰ BD 00, BD 03, BD 27, BD 44, BD 46, BD 58, BD 66, GOODS i6 0, UDF PFs i0, UDF PFs i4, UDF PFs IDROP1, UDF PFs1 i9 (Table 4 of Dow-Hygelund et al. 2007).

and $X_{\text{Ly}\alpha}^{55} = 8 \pm 8\%$ (1/13) at $z \sim 6$, consistent with Stark et al. (2011). Since they would not change so much the extrapolations derived by Stark et al. (2011) due to the large statistical uncertainties of the combined results, we do not calculate extrapolations using the combined results as well as the results of Stark et al. (2011).

Fontana et al. (2010) reported spectroscopic observation of seven z -dropout galaxies, with six having bright UV continua ($-21.75 < M_{\text{UV}} < -20.25$), and the other one having faint UV continuum ($-20.25 < M_{\text{UV}} < -18.75$). One of their galaxies shows Ly α emission with $EW_0 = 13\text{\AA}$. Furthermore, Vanzella et al. (2011) performed spectroscopic observations of two z -dropout candidates. Both of them have $M_{\text{UV}} < -20.25$ and the two galaxies show Ly α emission with EWs of 64 \AA and 50 \AA . Schenker et al. (2011) showed the results of spectroscopic observations of 19 galaxy candidates at $6.3 < z < 8.8$ selected by their photometric redshift technique (McLure et al. 2011). They reported three Ly α detections with EWs of 65 \AA , 65 \AA , and 30 \AA . Pentericci et al. (2011) presented the results of their spectroscopy for 11 z -dropout candidates, among which one galaxy is considered to be an interloper because of its multiple line detection. Seven galaxies have bright UV continua, while the remaining three galaxies are faint. Although two of the 10 candidates show Ly α detection, their Ly α EWs are lower than 25 \AA . Note that Ly α EW detection limits for the objects of Pentericci et al. (2011) is well below $EW_0^{Ly\alpha} = 25\text{\AA}$. Table 5 summarizes the spectroscopic results of z -dropout galaxies by Fontana et al. (2010), Vanzella et al. (2011), Schenker et al. (2011), and Pentericci et al. (2011). Schenker et al. (2011) estimated the Ly α fraction based on their results and the results of Fontana et al. (2010), correcting the effects of instrumentally-limited Ly α visibilities in wavelength and strong OH airglow lines. They obtained $X_{\text{Ly}\alpha}^{25} = 8.6_{-7.4}^{+8.4}\%$ for UV-bright galaxies and $X_{\text{Ly}\alpha}^{25} = 24 \pm 14\%$ for UV-faint galaxies. We estimate the Ly α fraction of z -dropout galaxies from Vanzella et al. (2011) and Pentericci et al. (2011) to be $X_{\text{Ly}\alpha}^{25} = 22_{-17}^{+18}\%$ (2/9) and $X_{\text{Ly}\alpha}^{55} = 11_{-11}^{+12}\%$ (1/9) for UV-bright galaxies at $z \sim 7$. For UV-faint galaxies, the upper limit of the Ly α fraction is $X_{\text{Ly}\alpha}^{25} < 33\%$ (0/3) and $X_{\text{Ly}\alpha}^{55} < 33\%$ (0/3). Comparing estimates of the Ly α fraction for $z \sim 7$ galaxies here, we find a spread due to small number statistics and possible field-to-field variation. Therefore, to minimize the Poisson noise and cosmic variance, we combine estimates of Ly α fraction from these independent studies. Combining these estimates assumes that the field-to-field variation is due to cosmic variance, and is not indicative of patchy reionization.

We now combine our results for $z \sim 7$ galaxies here with those from Fontana et al. (2010), Vanzella et al. (2011), Pentericci et al. (2011), and Schenker et al. (2011), to measure the Ly α fraction using the spectra of z -dropout galaxies obtained by three different groups. For the objects of Schenker et al. (2011), we use 14 objects whose redshifts are in the range of $6.3 < z < 7.3$, and take into account their correction factors for Ly α visibilities. Using the combined data, we calculate number-weighted mean Ly α fractions: $X_{\text{Ly}\alpha}^{25} = 17_{-9}^{+10}\%$ and

$X_{\text{Ly}\alpha}^{55} = 4 \pm 4\%$ for UV-bright galaxies, and $X_{\text{Ly}\alpha}^{25} = 24 \pm 12\%$ and $X_{\text{Ly}\alpha}^{55} = 16 \pm 9\%$ for UV-faint galaxies. In Figure 8, we present the evolution of Ly α fraction with redshift for LBGs over the range $4 < z < 7$. We also show, as shaded area, an extrapolation of lower- z Ly α fraction to $z \sim 7$, which is derived by Stark et al. (2011). We find that the Ly α fractions $X_{\text{Ly}\alpha}^{25}$ drop from $z \sim 6$ to 7 based on the combined results. These findings are similar to those reported by Schenker et al. (2011) and Pentericci et al. (2011).

Stark et al. (2010) reported that Ly α fraction increases with redshift over $3 < z < 6$ at fixed luminosity, and the trend is likely governed by redshift-dependent variations in dust obscuration, with additional contributions from kinematics and covering fraction of neutral hydrogen. In contrast to this increasing tendency of Ly α fraction from $z \sim 3$ to 6, we have found a significant drop of Ly α fraction from $z \sim 6$ to 7. This significant drop would suggest that Ly α emission lines from $z \sim 7$ galaxies are scattered by the IGM whose neutral hydrogen fraction is higher than that at $z \sim 6$. We would witness the increase of neutral hydrogen fraction toward $z \sim 7$ in the cosmic reionization history.

In Figure 8, we find that $X_{\text{Ly}\alpha}^{25}$ drops more strongly in the faint ($M_{\text{UV}} \simeq -19.5$) galaxies than in the bright ($M_{\text{UV}} \simeq -21$) galaxies; $X_{\text{Ly}\alpha}^{25}(z = 7; \text{obs}) / X_{\text{Ly}\alpha}^{25}(z = 7; \text{exp}) = 0.36 \pm 0.18$, and 0.53 ± 0.33 , respectively, where $X_{\text{Ly}\alpha}^{25}(z = 7; \text{obs})$ is the observed Ly α fraction at $z = 7$, and $X_{\text{Ly}\alpha}^{25}(z = 7; \text{exp})$ is the expected Ly α fraction at $z = 7$ derived by extrapolating the trend seen in lower redshifts to $z \sim 7$. This magnitude dependence of $X_{\text{Ly}\alpha}^{25}$ evolution could be explained by different halo masses of galaxies and the surrounding IGM. Given that the clustering strength of dropout galaxies increases with their UV luminosity (e.g., Giavalisco & Dickinson 2001; Ouchi et al. 2004; Adelberger et al. 2005; Lee et al. 2006), our results imply that the ionizing state of the IGM around galaxies hosted by less-massive dark matter halos changes later than that around galaxies hosted by massive dark matter halos. This would suggest that reionization proceeds from high- to low-density environments (inside-out; e.g., Ciardi & Madau 2003; Sokasian et al. 2002; Iliev et al. 2006, c.f., Finlator et al. 2009) rather than from low- to high-density regions (outside-in; e.g., Gnedin 2000; Miralda-Escudé et al. 2000).

We compare our composite results with those of model predictions derived by Dijkstra et al. (2011), which quantify the probability distribution function (PDF) of the fraction of Ly α photons transmitted through the IGM, by combining galactic outflow models with large-scale seminumeric simulations of reionization. They assume that the IGM at $z = 6$ was fully transparent to Ly α photons, and that the observed PDF for $\text{EW}_0^{\text{Ly}\alpha}$ at $z = 7$ is different only because of evolution of the ionization state of the IGM. Figure 9 compares their models with our composite results. Our results can be explained by an evolution of the neutral hydrogen fraction x_{HI} between $z = 6$ and 7; x_{HI} is roughly 0.6–0.9 at $z \sim 7$, which is similar to those reported by Schenker et al. (2011) and Pentericci et al. (2011).

The above discussion assumes that the dropout sam-

ples at different redshifts have similarly low contamination fractions from interlopers. We should, however, keep in mind that this assumption has not yet been justified well, although for the $z = 4 - 6$ UV-faint samples, Stark et al. (2010) estimated the contamination rate to be only 2 – 5 percent (c.f., Stanway et al. 2008; Douglas et al. 2009). Another possible source of systematic errors in our Ly α fraction analysis is inhomogeneities among the dropout samples in the spectroscopic detection limit and in the quality of the photometry used to estimate UV continua, both of which are difficult to fully take into account in our analysis. To reduce such inhomogeneities, desirable is a systematic spectroscopic survey over an entire redshift range combined with deep photometry redward of Ly α wavelength.

6. CONCLUSIONS

In this paper, we have presented Keck/DEIMOS spectroscopic observations of 11 z -dropout galaxies found in the SDF and GOODS-N fields. An emission line has been detected at 9500–10000Å in the spectra of three objects, one of which is the previously reported Ly α emitter IOK-1 at $z = 6.96$. Since all the detected lines are singlet with a large positive weighted skewness, we have concluded that the three objects are Ly α -emitting z -dropout galaxies at $z_{\text{spec}} = 7.213, 6.965$, and 6.844 . Their Ly α fluxes and rest-frame Ly α EWs are $2.5 \times 10^{-17} \text{ erg s}^{-1} \text{ cm}^{-2}$ and 33Å, $2.8 \times 10^{-17} \text{ erg s}^{-1} \text{ cm}^{-2}$ and 43Å, $2.7 \times 10^{-17} \text{ erg s}^{-1} \text{ cm}^{-2}$ and 43Å, respectively. It should be noted that the $z = 7.213$ galaxy was confirmed by observations in two independent DEIMOS runs in 2010 and 2011 with three different spectroscopic configurations. This galaxy is detected in HST/WFC3 F140W imaging as well as in Spitzer/IRAC 3.6 and 4.5 μm imaging. Stellar population modeling indicates that this galaxy has a very young age, a stellar mass $\lesssim 10^9 M_{\odot}$, and a high star formation rate of $30 - 100 M_{\odot} \text{ yr}^{-1}$, with strong nebular emission contributing to the fluxes in the IRAC bands.

We then have measured the fraction of Ly α -emitting galaxies at $z \sim 7$. To reduce statistical uncertainties and possible effects of field-to-field variance, we have combined our results with previous z -dropout spectroscopic studies (Fontana et al. 2010; Vanzella et al. 2011) including very recent ones (Schenker et al. 2011; Pentericci et al. 2011). We have obtained the $z \sim 7$ Ly α fraction of $X_{\text{Ly}\alpha}^{25} = 17 \pm 10\%$, and $X_{\text{Ly}\alpha}^{55} = 4 \pm 4\%$ for UV-bright galaxies ($-21.75 < M_{\text{UV}} < -20.25$, or $M_{\text{UV}} \simeq -21$), and $X_{\text{Ly}\alpha}^{25} = 24 \pm 12\%$, and $X_{\text{Ly}\alpha}^{55} = 16 \pm 9\%$ for UV-faint galaxies ($-20.25 < M_{\text{UV}} < -18.75$, or $M_{\text{UV}} \simeq -19.5$). These low values indicate that the fraction of Ly α -emitting galaxies drops from $z \sim 6$ to 7, in contrast to the reported increasing trend from $z \sim 4$ to 6. We have also found that $X_{\text{Ly}\alpha}^{25}$ drops more strongly in UV-faint galaxies than in UV-bright galaxies. These findings would suggest that the neutral fraction of the IGM significantly increases from $z \sim 6$ to 7, and that the increase is stronger around galaxies with fainter UV luminosities, which is consistent with inside-out reionization models where reionization proceeds from high- to low-density environments.

ACKNOWLEDGEMENTS

We thank the anonymous referee for valuable comments and suggestions which improved the manuscript. The authors wish to recognize and acknowledge the very significant cultural role and reverence that the summit of Mauna Kea has always had within the indigenous Hawaiian community. We are most fortunate to have the opportunity to conduct observations from this mountain. We would like to thank Michael Cooper and Yousuke Utsumi for giving us helpful advices to reduce DEIMOS spectra. We are also thankful to Richard Ellis for giving us helpful comments on an early draft of this paper,

and to Mark Dijkstra for providing us with the machine-readable table of their simulation results. Y.O. acknowledges support from the Japan Society for the Promotion of Science (JSPS) through the JSPS Research Fellowship for Young Scientists. The work of DS was carried out at Jet Propulsion Laboratory, California Institute of Technology, under a contract with NASA. H.S. would like to acknowledge the support of the National Science Foundation during the earlier phases of his spectroscopic program at the Keck Observatory.

Facilities: Subaru (Suprime-Cam), Keck (DEIMOS).

REFERENCES

- Adelberger, K. L., Steidel, C. C., Pettini, M., Shapley, A. E., Reddy, N. A., & Erb, D. K. 2005, *ApJ*, 619, 697
- Atek, H., et al. 2010, *ApJ*, 723, 104
- Bouwens, R. J., et al. 2010a, *ApJ*, 709, L133
- . 2010b, *ApJ*, 708, L69
- . 2011a, *Nature*, 469, 504
- . 2011b, *ApJ*, 737, 90
- Bradley, L. D., et al. 2011, *ArXiv e-prints (arXiv:1104.2035)*
- Bruzual, G., & Charlot, S. 2003, *MNRAS*, 344, 1000
- Bunker, A. J., et al. 2010, *MNRAS*, 409, 855
- Cai, Z., et al. 2011, *ApJ*, 736, L28+
- Calzetti, D., Armus, L., Bohlin, R. C., Kinney, A. L., Koornneef, J., & Storchi-Bergmann, T. 2000, *ApJ*, 533, 682
- Castellano, M., et al. 2010a, *A&A*, 511, A20+
- . 2010b, *A&A*, 524, A28+
- Ciardi, B., & Madau, P. 2003, *ApJ*, 596, 1
- Davis, M., et al. 2003, in *Society of Photo-Optical Instrumentation Engineers (SPIE) Conference Series*, Vol. 4834, *Society of Photo-Optical Instrumentation Engineers (SPIE) Conference Series*, ed. P. Guhathakurta, 161–172
- Dayal, P., Ferrara, A., & Gallerani, S. 2008, *MNRAS*, 389, 1683
- Dayal, P., Ferrara, A., Saro, A., Salvaterra, R., Borgani, S., & Tornatore, L. 2009, *MNRAS*, 400, 2000
- Dayal, P., Maselli, A., & Ferrara, A. 2011, *MNRAS*, 410, 830
- Dijkstra, M., Lidz, A., & Wyithe, J. S. B. 2007, *MNRAS*, 377, 1175
- Dijkstra, M., Mesinger, A., & Wyithe, J. S. B. 2011, *MNRAS*, 414, 2139
- Douglas, L. S., Bremer, M. N., Lehnert, M. D., Stanway, E. R., & Milvang-Jensen, B. 2010, *MNRAS*, 409, 1155
- Douglas, L. S., Bremer, M. N., Stanway, E. R., Lehnert, M. D., & Clowe, D. 2009, *MNRAS*, 400, 561
- Dow-Hygelund, C. C., et al. 2007, *ApJ*, 660, 47
- Dunkley, J., et al. 2009, *ApJS*, 180, 306
- Dunlop, J. S., McLure, R. J., Robertson, B. E., Ellis, R. S., Stark, D. P., Cirasuolo, M., & de Ravel, L. 2011, *ArXiv e-prints (arXiv:1102.5005)*
- Erb, D. K., Steidel, C. C., Shapley, A. E., Pettini, M., Reddy, N. A., & Adelberger, K. L. 2006, *ApJ*, 647, 128
- Faber, S. M., et al. 2003, in *Presented at the Society of Photo-Optical Instrumentation Engineers (SPIE) Conference*, Vol. 4841, *Society of Photo-Optical Instrumentation Engineers (SPIE) Conference Series*, ed. M. Iye & A. F. M. Moorwood, 1657–1669
- Fan, X., et al. 2006, *AJ*, 132, 117
- Finkelstein, S. L., Papovich, C., Giallisco, M., Reddy, N. A., Ferguson, H. C., Koekemoer, A. M., & Dickinson, M. 2010, *ApJ*, 719, 1250
- Finlator, K., Özel, F., Davé, R., & Oppenheimer, B. D. 2009, *MNRAS*, 400, 1049
- Fontana, A., et al. 2010, *ApJ*, 725, L205
- Furlanetto, S. R., Zaldarriaga, M., & Hernquist, L. 2006, *MNRAS*, 365, 1012
- Giallisco, M. 2002, *ARA&A*, 40, 579
- Giallisco, M., & Dickinson, M. 2001, *ApJ*, 550, 177
- Giallisco, M., et al. 2004, *ApJ*, 600, L93
- Gnedin, N. Y. 2000, *ApJ*, 535, 530
- González, V., Labbé, I., Bouwens, R. J., Illingworth, G., Franx, M., & Kriek, M. 2011, *ApJ*, 735, L34+
- González, V., Labbé, I., Bouwens, R. J., Illingworth, G., Franx, M., Kriek, M., & Brammer, G. B. 2010, *ApJ*, 713, 115
- Goto, T., Utsumi, Y., Hattori, T., Miyazaki, S., & Yamauchi, C. 2011, *MNRAS*, 415, L1
- Grazian, A., et al. 2011, *A&A*, 532, A33+
- Haiman, Z., & Cen, R. 2005, *ApJ*, 623, 627
- Haiman, Z., & Spaans, M. 1999, *ApJ*, 518, 138
- Hickey, S., Bunker, A., Jarvis, M. J., Chiu, K., & Bonfield, D. 2010, *MNRAS*, 404, 212
- Hu, E. M., Cowie, L. L., Capak, P., McMahon, R. G., Hayashino, T., & Komiyama, Y. 2004, *AJ*, 127, 563
- Hu, E. M., Cowie, L. L., & McMahon, R. G. 1998, *ApJ*, 502, L99+
- Iliev, I. T., Mellema, G., Pen, U.-L., Merz, H., Shapiro, P. R., & Alvarez, M. A. 2006, *MNRAS*, 369, 1625
- Iliev, I. T., Shapiro, P. R., McDonald, P., Mellema, G., & Pen, U. 2008, *MNRAS*, 391, 63
- Iye, M., et al. 2006, *Nature*, 443, 186
- Kajisawa, M., et al. 2011, *PASJ*, 63, 379
- Kakazu, Y., Cowie, L. L., & Hu, E. M. 2007, *ApJ*, 668, 853
- Kashikawa, N., et al. 2004, *PASJ*, 56, 1011
- . 2006, *ApJ*, 648, 7
- . 2011, *ApJ*, 734, 119
- Kennicutt, Jr., R. C. 1998, *ARA&A*, 36, 189
- Kobayashi, M. A. R., Totani, T., & Nagashima, M. 2007, *ApJ*, 670, 919
- Komatsu, E., et al. 2011, *ApJS*, 192, 18
- Labbé, I., et al. 2010, *ApJ*, 708, L26
- Larson, D., et al. 2011, *ApJS*, 192, 16
- Lee, K.-S., Giallisco, M., Gnedin, O. Y., Somerville, R. S., Ferguson, H. C., Dickinson, M., & Ouchi, M. 2006, *ApJ*, 642, 63
- Lehnert, M. D., et al. 2010, *Nature*, 467, 940
- Lorenzoni, S., Bunker, A. J., Wilkins, S. M., Stanway, E. R., Jarvis, M. J., & Caruana, J. 2011, *MNRAS*, 414, 1455
- Madau, P. 1995, *ApJ*, 441, 18
- Madau, P., Pozzetti, L., & Dickinson, M. 1998, *ApJ*, 498, 106
- Malhotra, S., & Rhoads, J. E. 2004, *ApJ*, 617, L5
- Markwardt, C. B. 2009, in *Astronomical Society of the Pacific Conference Series*, Vol. 411, *Astronomical Society of the Pacific Conference Series*, ed. D. A. Bohlender, D. Durand, & P. Dowler, 251+
- McCarthy, P. J. 1993, *ARA&A*, 31, 639
- McLure, R. J., Dunlop, J. S., Cirasuolo, M., Koekemoer, A. M., Sabin, E., Stark, D. P., Targett, T. A., & Ellis, R. S. 2010, *MNRAS*, 403, 960
- McLure, R. J., et al. 2011, *ArXiv e-prints (arXiv:1102.4881)*
- McQuinn, M., Hernquist, L., Zaldarriaga, M., & Dutta, S. 2007, *MNRAS*, 381, 75
- Mesinger, A., & Furlanetto, S. R. 2008, *MNRAS*, 386, 1990
- Mesinger, A., Haiman, Z., & Cen, R. 2004, *ApJ*, 613, 23
- Miralda-Escudé, J., Haehnelt, M., & Rees, M. J. 2000, *ApJ*, 530, 1
- Nagao, T., Maiolino, R., & Marconi, A. 2006, *A&A*, 447, 863
- Nakamura, E., Inoue, A. K., Hayashino, T., Horie, M., Kousai, K., Fujii, T., & Matsuda, Y. 2011, *MNRAS*, 412, 2579
- Oesch, P. A., et al. 2010, *ApJ*, 709, L16
- . 2011, *ArXiv e-prints (arXiv:1105.2297)*
- Oke, J. B., & Gunn, J. E. 1983, *ApJ*, 266, 713
- Ono, Y., Ouchi, M., Shimasaku, K., Dunlop, J., Farrah, D., McLure, R., & Okamura, S. 2010, *ApJ*, 724, 1524
- Ouchi, M., et al. 2004, *ApJ*, 611, 685
- . 2008, *ApJS*, 176, 301
- . 2009, *ApJ*, 706, 1136
- . 2010, *ApJ*, 723, 869

- Pentericci, L., et al. 2011, ArXiv e-prints (arXiv:1107.1376)
- Pettini, M., Shapley, A. E., Steidel, C. C., Cuby, J., Dickinson, M., Moorwood, A. F. M., Adelberger, K. L., & Giavalisco, M. 2001, *ApJ*, 554, 981
- Raiter, A., Fosbury, R. A. E., & Teimoorinia, H. 2010, *A&A*, 510, A109+
- Reddy, N. A., Steidel, C. C., Pettini, M., Adelberger, K. L., Shapley, A. E., Erb, D. K., & Dickinson, M. 2008, *ApJS*, 175, 48
- Rhoads, J. E., Malhotra, S., Dey, A., Stern, D., Spinrad, H., & Jannuzi, B. T. 2000, *ApJ*, 545, L85
- Rhoads, J. E., et al. 2003, *AJ*, 125, 1006
- Salpeter, E. E. 1955, *ApJ*, 121, 161
- Santos, M. R., Ellis, R. S., Kneib, J., Richard, J., & Kuijken, K. 2004, *ApJ*, 606, 683
- Schaerer, D., & de Barros, S. 2009, *A&A*, 502, 423
- . 2010, *A&A*, 515, A73+
- Schenker, M. A., Stark, D. P., Ellis, R. S., Robertson, B. E., Dunlop, J. S., McLure, R. J., Kneib, J. ., & Richard, J. 2011, ArXiv e-prints (arXiv:1107.1261)
- Shapley, A. E., Steidel, C. C., Pettini, M., & Adelberger, K. L. 2003, *ApJ*, 588, 65
- Shim, H., Chary, R.-R., Dickinson, M., Lin, L., Spinrad, H., Stern, D., & Yan, C.-H. 2011, *ApJ*, 738, 69
- Shimasaku, K., et al. 2006, *PASJ*, 58, 313
- Sokasian, A., Abel, T., & Hernquist, L. 2002, *MNRAS*, 332, 601
- Stanway, E. R., Bremer, M. N., & Lehnert, M. D. 2008, *MNRAS*, 385, 493
- Stanway, E. R., et al. 2007, *MNRAS*, 376, 727
- Stark, D. P., Ellis, R. S., Chiu, K., Ouchi, M., & Bunker, A. 2010, *MNRAS*, 408, 1628
- Stark, D. P., Ellis, R. S., & Ouchi, M. 2011, *ApJ*, 728, L2+
- Steidel, C. C., Erb, D. K., Shapley, A. E., Pettini, M., Reddy, N., Bogosavljević, M., Rudie, G. C., & Rakic, O. 2010, *ApJ*, 717, 289
- Steidel, C. C., Giavalisco, M., Pettini, M., Dickinson, M., & Adelberger, K. L. 1996, *ApJ*, 462, L17+
- Stern, D., Yost, S. A., Eckart, M. E., Harrison, F. A., Helfand, D. J., Djorgovski, S. G., Malhotra, S., & Rhoads, J. E. 2005, *ApJ*, 619, 12
- Vanzella, E., et al. 2009, *ApJ*, 695, 1163
- . 2010, *A&A*, 513, A20+
- . 2011, *ApJ*, 730, L35+
- Wilkins, S. M., Bunker, A. J., Ellis, R. S., Stark, D., Stanway, E. R., Chiu, K., Lorenzoni, S., & Jarvis, M. J. 2010, *MNRAS*, 403, 938
- Wilkins, S. M., Bunker, A. J., Lorenzoni, S., & Caruana, J. 2011, *MNRAS*, 411, 23
- Yan, H., Windhorst, R. A., Hathi, N. P., Cohen, S. H., Ryan, R. E., O'Connell, R. W., & McCarthy, P. J. 2010, *Research in Astronomy and Astrophysics*, 10, 867
- Yan, H., et al. 2011, *ApJ*, 728, L22+